Numerical Studies on Dynamic Behaviour of Tubular T-joint Subjected to Impact Loading

Hui Qu[a]; **Jingsi Huo[b]; Chao Xu[a]; Feng Fu[c]

[a]*School of Civil Engineering, Yantai University, Yantai, 264005, China*
[b]*China Ministry of Education Key Laboratory of Building Safety and Energy Efficiency, College of Civil Engineering, Hunan University, Yuelu Mountain, Changsha, 410082, China*
[c]*School of Engineering and Mathematical Sciences, City University London, Northampton Square, London,EC1V 0HB*

Abstract: Joints play an important role in resisting impact loading in Tubular structures. In this paper, a finite element model validated by experimental results is developed to numerically study the failure modes and buckling mechanism of tubular T-joint impacted by a drop hammer with the initial velocity of 7-10 m/s. The resistant mechanism is investigated based on the dynamic responses of the joints under impact loading. Strain, displacement and the failure modes of the T-joints are also predicted. Global and local deformations of the tubular joints are distinguished using an equal area axis method, which helps to discover the buckling mechanism of the joints. Using the yield line theory, , an equivalent impact force estimation method is also proposed based on the impact load versus displacement relationship. The numerical analysis and the simplified method provide a basis for impact resistance evaluation and progressive collapse mitigation of steel tubular structures in design practice in the future.

Keywords: tubular T-joint, impact loading, numerical analysis, buckling mechanism, equivalent impact force estimation method

** Please address all correspondence to Professor Jingsi Huo, Tel: 86 731 88821447, Fax: 86 731 88821395, E-mail: jingsihuo@gmail.com

1. Introduction

Tubular structure is load bearing structural system widely used in offshore jacket platform or breakwater due to its excellent axial loads resistance, lower response

to fluid flow and fast track construction, transportation and erection. During its service period, it may be subjected to impact loads, such as the ship collision, floating iceberg collision, or explosion and fire resulted from leaking oil and gas. The pioneer research work on the impact behaviours of tubular structure can be traced back to Spares and Soreide [1]. They developed a rigid-plastic analytical formulation for the analysis of laterally loaded tubular members with various boundary conditions and different load distributions. Henceforth, Zeinoddini et al. ([2]-[7]), Chen and Shen [8], Bambach et al. [9] and Jones et al. [10,11] performed some experimental and analytical studies on the dynamic behaviours of steel tubular members under impact loading. The literatures [2-11] focused mainly on the effects of geometric parameters, loading condition and boundary condition on the dynamic loads, deformational and energy-absorption behaviors and failure mechanism of steel tubular members. Based on the above experimental and numerical analyses, some simple formulas were proposed to determine the ultimate load-bearing capacity and divide the local and global deformations or deformational energies.

The tubular joints are the critical structural components which play an important role in transferring load in the tubular structure. However, few tests and numerical studies had been reported to analyze the dynamic behaviors of tubular joints or tubular structures under impact loading. Jin et al. [12] presented a non-linear dynamic analysis procedure for simulating the

dynamic responses of a tubular platform structure under impact action based on the forensic evidence from the damaged components, and then evaluating the global damage effects on the platform structure. Wang et al. [13] compared the impact resistance of reinforced and unreinforced tubular K-joints. Yu et al. [14] performed experimental study on mechanical behavior of steel tubular T-joint in fire and impact loading. Qu et al. ([15]-[17]) carried out a series of numerical studies on the dynamic behaviors of tubular T-joint under different impact loading conditions, which were aimed to discover the failure modes and impact resistant mechanism of tubular T-joints.

The impact tests and numerical analysis described in the above literatures generally focus on the failure modes and load-bearing capacity of steel tubes and tubular joints. The impact loading is generally applied by a free-falling drop hammer. Due to the instantaneous characteristic of the impact loading, the dynamic response of structure under impact loading is evidently different to that under static loading and is difficult to be recorded completely during the tests. This paper aims at the experimental and numerical analysis of the dynamic behaviour of tubular T-joint under impact loading. A finite element model is developed and is validated by the impact tests conducted by the authors. Numerical analysis of the failure mechanism of steel tubular T-joints under impact loading is also conducted. The local indentation of the chord is distinguished from the global deformations of the T-joints through an equal area axis method and the yield line theory. Finally, an equivalent impact force estimation method is proposed to determine the anti-impact resistance of steel tubular T-joint.

2. Finite element modeling

A finite element model is developed here to simulate the dynamic behaviour of steel tubular T-joint under impact loading using the general purpose program ABAQUS 6.10 [18]. Figure 1 shows the three dimensional finite element model of the tubular T-joint. It replicates the full scale tests which are to be described in Section 3. The drop hammer, brace, chord and rigid plates are simulated using 8-node 3D reduced-integration solid elements (C3D8R). The meshes of the chord in the brace-chord connecting zone are refined to improve the accuracy of the FE analysis. The rigid plate at both ends of chord is simply supported at the center axis and the top end of brace is free. The drop hammer is modeled as a rigid cylinder with the height of 400 mm and the diameter of 180 mm. The cylinder is placed on the top surface of brace with the axis of them coincides. Different impact energies (as shown in Table 1) are applied by changing the weight of the hammer. An initial velocity, ranging from 7 to10 m/s, is applied to the drop hammer at the beginning of impact testing.

As no weld fracture was observed in the impact tests conducted by Qu and Huo [19], which will be described in Section 4, so, a “Tie Contact” from ABAQUS library is used to simulate the connection between the brace and the chord. “Self Contact” from ABAQUS is used to simulate the contact behaviour between the hammer and the top cover plate of the brace during impact loading.

An explicit dynamic procedure is used to solve the non-linear equilibrium equations of motion for the impact analysis.

Under static load, the idealized uniaxial stress-strain relationship of mild steel (as shown in Figure 2) is used to represent the elastic-perfectly plastic behavior of steel. As the yield stress

of steel under dynamic loading is sensitive to strain rate[20], the dynamic flow stress of steel increases with an increase of strain rate. The Cowper-Symonds constitutive equation is used here to simulate the strain-rate sensitive behaviour of steel under impact loading. The Cowper-Symonds constitutive equation is expressed as follow:

$$\sigma_{dy} = \sigma_y (1 + (\frac{\dot{\varepsilon}}{D})^{\frac{1}{n}}) \tag{1}$$

where σ_{dy} is the dynamic yield stress at a uniaxial plastic strain rate, σ_y is the associated static yield stress, and $\dot{\varepsilon}$ is strain rate for steel, D is a rate-dependent constant and n is a positive dimensionless parameter. According to the literature (Abramowicz and Jones [20]), D = 40 s^{-1} and n = 5 for mild steel.

3. Experimental programme

A series of tests on tubular T-joint under impact loading has been conducted by Qu and Huo [19], and some of the test results are used herein to validate the FE model proposed in this paper.

3.1 Specimen material and fabrication

Four tubular T-joints are tested using the drop hammer test machine at the Center for Integrated Protection Research of Engineering Structures (CIPRES), Hunan University. The test parameters were impact energy (E), length to radius ratio of chord (α) and diameter of chord (D). The details of each specimen is listed in Table 1, where D, T, L are the diameter, thickness and effective length of the chord, respectively; d, t, l are the diameter, thickness and

length of the brace, respectively. *m* and *v* represent the weight and impact velocity of drop hammer respectively.

The chords and braces of four specimens are made from a 6-7m long cold-formed seamless steel tube and fully welded together. Three 6mm thick steel cover plates are welded to both the ends of the chord and the top end of the brace respectively.

Strips coupons cut from of the steel tubes were tested in tension. The test results show that the yield strength (f_y) of 4mm, 6mm, and 7mm thick steel plates are 492MPa, 499MPa and 445MPa respectively, and the ultimate strength are 553MPa, 596MPa and 525MPa respectively.

3.2 Test setup

Five strain gauges are mounted onto the connection zone between brace and chord to monitor the strain development during the impact loading. The “sad”, “crn”, “bot”, “maxa” and “maxc” stand for saddle point, crown point, the bottom of chord, axial and circumferential direction of maximum deformed position in the section respectively. Two displacement transducers are used to measure the vertical displacements of the free end of the brace and the bottom of the mid-span of the chord. A load cell is embodied into the drop hammer to record the time history of impact force. The details of specimens, strain gauge layout, and arrangement of test setup are shown in Figure 3 and Figure 4.

4. Verification of the nonlinear FE model

The FE model was used to simulate the failure modes, dynamic responses of impact loads, lateral displacements and to predict the dissipated energy of the tubular T-joint. It is validated against the test in section 3. The comparisons of the numerical results with the experimental results are shown as follows.

4.1 Failure modes

Figure 5 shows the comparisons between the numerical modeling and experimental results in the terms of failure modes of tubular joints under different impact energies. It can be seen that the numerical results agree well with the experimental results. The failure modes indicate that all the specimens fail due to the remarkable local indentation of the chord at the position close to the joints and also due to the subsequent global bending of the chord.

From the comparisons shown in Table 1 and Figure 5, it can be seen that Specimens J14a (E_k=11.2kJ, Figure 5-a(2)), J15a (E_k=14.5kJ, Figure 5-b(2)) and J14b (E_k=23kJ, Figure 5-c(2)) experienced different failure modes due to different impact energies. With the increase of impact energies, the failure modes of the three joints change from light local dent on the top surface of chord into severe local dent coupled with evident flexural buckling at the middle span of the chord. Although Specimen J35b (E_k=29.5kJ, Figure 5-d(2)) is loaded to failure under a larger impact energy, the failure mode is local indentation of the top surface of chord and slight global buckling, which is similar to that of Specimen J14a. The locally buckled

zone is in an elliptical shape.

Figure 6 shows the comparison of failure mode of the chord cross-section of Specimen J15a between test and simulation result. It can be seen that the deformed cross-section looks like a double layer bowl after the testing and the simulated deformed cross section is in good agreement with the test result.

4.2 Dynamic responses of T-joint

Due to accident of the data logger system during the tests, the test resullt of Specimen J14b were not captured. As it is well known, as soon as the hammer hit the top end of brace, the elastic stress wave starts to develop. With the stress wave travelling in the joint and hammer, the joints were deforming successively. At the same time, the signanals recorded by the load cell embodied in the hammer, displacement transducers and strain gauges ringed to some extent, so there are a serial of different fluctuations in the history response of impact load, displacement, and strain.

The time history responses of impact load of Specimens J14a, J15a and J35b from numerical simulation (shown in Figure 7) agree well with the experimental results. The time history responses from both the simulation and the experimental results can be used to reveal the impact load resistance mechanism and deformational behaviour. By analyzing the time history curves obtained from numerical analysis and experimental tests, it can be seen that it can be divided into three stages. Firstly, the impact force goes up to the maximum value sharply in a very short period of time. After being loaded to the peak load, the impact load decreases

with sharp fluctuation during the second stage. Hereafter, the fluctuation gradually diminishes, therefore, the impact load versus time history curve tends to be flat and smooth. Finally, the impact load decreases to zero The predicted impact forces and impact duration time from the numerical analysis are slightly less than those of experimental results. In order to further analyse the failure mechanism, seven typical time points are selcted to highlight the deformational development of the tubular T-joint.

It can be seen from Figure 4 and Figure 1 that both ends of chord are placed on a circular steel cylinder in the test, while in the FE analysis, both ends of chord are constrained in X,Y,Z translation direction at central axis of the rigid plates to simulate the pin support. The axial constraint is more or less weaker in the test than that in the FE analysis, especially when the tubular joint suffers from a lateral load, which will lead the deflection measurement larger than that from the numerical simulation. Figure 8 shows the comparisons of vertical displacement at the top end of the brace in Specimens J14a and J15a. between the test results and numerical simulation. It can be seen that the numerical results are in generally matching the test results, However, the predicted ultimate displacements are higher than the test results.

Figure 9 shows the comparisons between the test results and numerical simulation in impact force versus displacement curves of Specimens J14a, J15a and J35b. The simulated peak impact forces of the three specimens are in good agreement with the test results with the deformation and initial impact resistance stiffness are slightly larger than those of

experimental results.

All the discrepancy between the numerical simulation and test results can be attributed to that (1) the hammer and end-plate of brace in the FE model are simplified as rigid body and it would lead to a shorter contact duration time between the hammer and brace. (2) In the tests, the ends of chord are connected to a rigid base frame with two steel rollers. The imperfection of the specimens and base supports would lead to some rotational restraint at the end connections of the T-joints. It is difficult to accurately evaluate the rotational restraint , therefore an idealized frictionless pin restrain is used in the FE model to represent the actual supports. Therefore, the test results would lead to a larger global bending stiffness of the specimens and smaller ultimate lateral displacement and larger impact force than the corresponding simulation results. Meanwhile, during the tests, the rotational restraint developed by the supports also dissipates some impact energy and it results smaller measured dissipated energy of the joint compared with the simulated results.

4.3 Time History of Strain

Figure 10 shows the comparisons of time history curves of strain between the test results and simulation results at typical locations where the strain gauges are mounted to Specimens J14a and J15a. The strain gauges maybe failed by fracture or gauge-to-steel interfacial debonding during test. It can be seen from Figure 10 that as the drastic deformation make some strain gauges fail at the beginning of impact, the measured time history of strain is short, and the measured strain changes more seriously than that of numerical results. But it also can be seen

that the FE model can accurately predict the dynamic strain responses of the tubular joints and the predicted result is slightly greater than the measured result in the initial phase of impact. In the tests the maximum longitudinal strain values measured generally exceed 0.01 and the circumferential strain values at the maximum deformation position in the cross section even reached 0.24.

Based on the above comparisons, it can be concluded that the proposed model is accurately enough to simulate the dynamic response of tubular joints under impact loading. Therefore, further analysis of the dynamic response of steel tubular joints is performed using the proposed FE model.

4.5 Energy transformation

In the tests, the steel tubular T-joints are loaded with impact loading and significant plastic deformation is observed which is locally confined to the connection zone between brace and chord. Figure 5 demonstrates the local indentation mode and global buckling mode under impact loading. The impact energies are mainly dissipated by plastic deformation of steel tube. The dissipated energies can be determined by calculating the area between the impact force versus displacement curve (as shown in Figure 9) along the horizontal coordinate. Moreover, the plastically dissipated energy can obtained directly from the FE modeling. The measured and simulated dissipated energy and the ratio of dissipated energy to applied impact energy are shown in Figure 11. Figure 11-(a) shows the plastic dissipation energies calculated from FE model which are in good agreement with the that from the test results. Figure 11-(b) shows

the ratios of the dissipated energy to the applied impact energy, which are almost constant within the experimental parameters.

5. Mechanism of Buckling in Tubular Joint under Impact Loading

5.1 Local and global deformation

It can be demonstrated from Figure 5 that the tubular joints under impact loading are subjected to both local and global deformations. The FE analysis indicates that the tubular joint experiences the coupled local and global deformations during the impact loading. The following FE analysis on Specimen J14a is conducted for further understanding of the deformational behaviour of tubular T-joints under impact loading. As shown in Figure 7, the impact loading lasts about 45ms. The seven time points of 0, 0.25, 0.5, 2.5, 23.5, 35 and 45ms are marked in the measured impact load versus time relation curves. The isometric views of deformed tubular joints and sectional views of both undeformed and deformed mid-span section of the chords corresponding to the seven time points are shown in Figure 12.

Figure 12-(1) illustrates the initial state of the tubular joint before being loaded. As shown in Figure 7, after the hammer touches the top of brace, the impact force reaches to a peak value at 0.25 ms. The stress in connection zone between the brace to chord is negligible and little deformation is found in the brace and chord at this stage as well, (as shown in Figure 12-(2)). This stage can be named as flexible response stage. The dynamic response in this stage

mainly is caused by hard contact between the hammer and the cover plate of the brace. As the impact force is transformed directly from top end of brace to the weld at the brace-chord intersection during the stage from 0.25ms to 0.5ms, it leads to a severe stress concentration close to the weld at the brace-chord intersection, especially at the saddle and crown points. After the wall of the tube in the vicinity of the brace-chord connecting zone yields, the area of steel tube close to the brace-chord intersection experiences local indentation and the chord suffers little global deformation during this stage, as shown in Figure 12-(3). The local indentation of steel tube makes the impact force decrease to point 2. With the development of impact loading, plastic deformation around the intersection weld is developed, which dissipates the impact energy. Accordingly, the local indentation and plastic yielding of the chord make the impact force to decrease to zero in a short duration of time, as shown Point 3 in Figure 7. Figure 12-(4) shows that the top surface of chord at mid-span section suffers prominent local indentation when the loading increases to Point 3. Subsequently, the impact force increases again and the top surface of the chord yields progressively when the impact force continues to fluctuate till to be stable at Point 4. In the stage the local indentation stabilizes while the global bending deformation increases remarkably, as shown in Figure 12-(5)-(a, b). The plateau phase ranging from Point 4 to 5 indicates that the chord of the tubular joint is suffering progressive global buckling, as shown in Figure 12-(6). The final stage ranging from Point 5 to 6 is the unloading stage, where the deformations of the tubular joint recover obviously, as shown in Figure 12-(7) and Figure 9.

5.2 Residual deformations

Distinguishing the local deformation from the global deformation correctly helps to better understand the dynamic behaviour of tubular T-joints under impact loading and establish the practical analysis method to evaluate the dynamic resistance against the impact loads. As the deformation shape of the tubular section under impact loading is complex, it is difficult to distinguish the local deformation from the global deformation. Jones and Brich [10] proposed a method to distinguish the local and global components of the total displacement measurement of the final cross-section. By idealizing the deformed tubular cross-section and calculating geometry relationship, the local and global deformations can be defined in Figure 13-(a). As the impact energy is transferred by the brace and the cross-sectional shape of brace affects the deformed cross-sectional shape of the chord at mid-span, the failure mechanism herein is different from that described in Jones and Brich [10]. The method proposed by Jones and Brich [10] cannot be used to analyze the deformations of the tubular T-joint. Numerical study shows that the distance between two equal area axes of undeformed and deformed chord is the global bending deformation. As the shape of deformed cross-section is irregular, it is difficult to calculate the position of equal area axis by using analytical method, the following numerical method is proposed in this paper.

The numerical method includes five steps: (1) the deformed cross sections at different characteristic times is selected on the basis of time history of numerical deformation; (2) to determine the coordinates of every point in the deformed section corresponding to each characteristic time; (3) to divide the section at characteristic time into n segments along axis y; (4) to search a horizontal axis that bisects the deformed cross-section giving equal area above

and below it., then the horizontal axis is named as the equal area axis of the deformed section , and the global deformations are defined as the distance between the x-axis of the undeformed cross-section and the equal area axis. In fact, the global displacement is the *y* coordinate of the equal area axis; (5) the local dent can be determined by deducting the global displacement from the total lateral displacement of drop hammer which is obtained by FEM method. The iteration method should be used in order to obtain the equal area axis.

The above iteration method can be used to determine the time history curves of local indentation and global bending displacement of the Specimens, as shown in Figure 14. The typical time points shown in Figure 7 are also introduced into Figure 14 in order to investigate the buckling mechanism of the tubular T-joint under impact loading. Chinese Code for design of steel structure (GB50017-2003)[21] requires that the dent depth of steel tube for the limit state of local indentation should be less than 0.03*D*, and the relative horizontal displacement for the strength limit state should not exceed *L*/70 (*L* is the span of beam or story height of column). It can be seen from Figure 14 that the local indentation failure significantly precedes the global buckling failure. The local dent of tubular T-joint increases quickly at the beginning of impact loading (before Point 3). The local indentation is dominant during the initial stage which corresponds to the fluctuating phase of the impact force versus time relation curve from Point 3 to 4. Therefore, the progressive local indentation on the steel tube near the brace to chord connection zone leads to the fluctuations on the impact force versus time relation curve. With the lapse of impact loading duration of time, for joint J14a and J35b with the failure mode of local indentation on the top surface of chord, the local deformation converges to a

certain value gradually, while the global bending displacement linearly increases and become predominant during the following impact loading duration of time. For the joint J15a and J14b with the failure mode of the coupled local and global deformations, the local deformation decreases with the global deformation increasing.

5.3 Strain rate and dynamic amplification coefficient

It can be found from the numerical analysis that the steel tube adjacent to the intersection weld suffers severe local deformation during impact loading. The local indentation mechanism makes the wall of the chord at the brace to chord connection zone suffer more extraordinary dynamic response, i.e. more obvious strain rate effect. The time history of the axial or circumferential strains at the saddle, crown, maximum transverse convex points and the chord bottom are differentiated in this paper to obtain the corresponding strain rate versus time relation curves showed in Figure 15.

The maximum strain rate of $15s^{-1}$ for the four joints is observed in the simulation. For the T-joints with the chord diameter of 180 mm, the strain rates at saddle and maximum transverse convex deformation in circumferential direction are larger than those at other locations. For Specimen J35b with the chord diameter of 325 mm, both maximum transverse convex deformations in axial and circumferential directions are larger than those at other positions. The dynamic yielding strength of steel was enhanced obviously due to strain rate effect. It can also be seen that all strain rate versus time relation curves at different positions change almost in the same way. The strain rate goes up to the peak gradually at the beginning

of strain rate versus time relation curve, and it decreases to zero at the end of impact loading. The peak value of the strain rate versus time relation curves illustrates the typical location where the steel tube suffers the severer local deformation. Generally, the strain rate at saddle and crown points reaches the peak first and the strain rate in the circumferential direction reaches the peak earlier than that in axial direction. The strain rate of chord bottom is always smaller than those of other positions. The phenomena can be attributed to that the saddle and crown points are close to the brace-chord weld and the impact force transformed from the brace causes severe deformation at the two points. With the development of impact loading, the buckled cross-section makes the stiffness of chord decrease and the bending deformation increase. Thus the strain rate at the maximum transverse deformation position changes dramatically and reaches to the peak quickly.

5.4 Impact force versus displacement curves

Impact force versus displacement curves of Specimens J14a, J15a and J35b are compared in Figure 16. Specimens J14a, J15a and J14b have same geometry parameters and are loaded under different impact energies. The similar impact force versus displacement relation curves with a steep descending branch and an evident strength degradation phase are shown in Fig.16. It can be seen that, the stronger the impact energy, the lower the ultimate impact force, the larger the deformation, and the severer the impact force degradation. Compared with Specimens J14a and J15a, Sepcimen J35b with a larger diameter of chord and a slightly larger impact energy suffers less local indentation and has a larger unloading stiffness. The measured dissipated energy can be determined by integrating the area enclosed by the impact force

versus displacement relation curve and the horizontal coordinate. The measured impact energies of the four specimens are shown in Table 2. It can be concluded from Table 2 that the increase of the diameter of chord leads to the increased dissipated energy due to the enlargement of the local indentation area.

5.5 Energy dissipation

Based on the equal-area axial method, the impact force versus local indentation relation curve of Specimen J15a is shown in Figure 17. Without considering energy loss during impact loading, the energy dissipated by local indentation and the energy dissipated by the total plastic deformation can be determined based on the test results shown in Figure 16 and Figure 17. Figure 18 demonstrates the numerical time history of the ratios of the local indentation-dissipated plus global bending-dissipated energy to the total plastic deformation energy of Specimen J15a during impact loading. It can be seen that, at the beginning of impact loading, local indentation becomes larger gradually and it dissipates about 35% of total deformation energy when the local deformation reaches the maximum value. Afterwards, as the effect of local deformation nearly does not change, the global deformation keeps increasing.

The energies dissipated by local indentation and the ratios of local indentation dissipated energy to the total dissipated energy for all specimens are shown in Figure 19. According to Figure 19 and Table 2, it can been seen that for Specimens J14a, J15a and J14b with the same geometrical parameters, increasing the impact energy leads to deeper local dent, shorter yield

line and more energy dissipated by local indentation. Then the global bending deformation increases and the ratio of local indentation-dissipated energy to the total dissipated energy decreases. Specimen J35b with a larger diameter is loaded to failure with the larger length of yield line and depth of local dent and the increased energy dissipation and ratio of local indentation dissipated energy to the total dissipated energy. The increased energy dissipation of Specimen J35b can be attributed to the fact that the larger diameter leads to the larger local indentation area and stronger flexural stiffness.

6. A simplified calculation method of impact resistance

It is imperative to develop a simplified calculation method to assess the impact resistance of tubular joint under possible extreme loading conditions. Some literatures [2-11] have addressed either analytical or numerical solutions to the impact resistance of tubular structure based on the experimental, analytical or numerical investigations. The research findings illustrate that some factors including the shape of striker, the impact position and the boundary conditions have significant effects on the impact resistance of tubular structure. Ellinas [22] developed a simple design-oriented analytical formula to estimate the reserve-load carrying capacity of circular tubular beam-column members with overall bending and local denting damage. Mohammad and Masoud [23] investigated the structural behavior of preloaded tubular members under lateral impact loads by means of finite element method. Three different kinds of end conditions have been applied to the model and the effects of boundary conditions are investigated. A relation between impact force and indent depth was put forward on the base of these analyses results.

In order to simplify the yield zone at the locally-buckled top surface of chord after test, the yield zone of experimental results is divided into four parts according to the yield line theory. The yield line pattern of the deformed top surface of chord is shown in Figure 20. The short-axis length is the distance between the two maximum transverse bulge points in the cross section of chord at mid-span and the long-axis length is the distance between the borders of dent on the longitudinal axis of top chord wall.

According to the approximate rigid-plastic analysis of shell intersections loaded dynamically described in Jones [24], the reciprocal theorem of work can be used to define the equivalent impact force (P_e) which leads to a certain dent depth on the top surface of chord.

$$DIF \cdot M_p \sum \theta_i l_i = P_e \Delta \tag{2}$$

where, *DIF* is the dynamic strength increase factor. The following dynamic increase factor (*DIF*) of steel, which is described in Malver and Ross [25], was adopted.

$$DIF = (\dot{\varepsilon}/10^{-4})^{(0.074-0.04 f_y/414)} \tag{3}$$

where, $\dot{\varepsilon}$ is strain rate of steel; f_y is the static yield strength of steel; M_p is the plastic moment of chord steel plate with a thickness of t, $m_p = f_y t^2/4$; Δ is the dent depth on the top surface of chord after failure; l_i is the length of yield line of part i; θ_i is the maximum rotation of plastic hinge i. For yield line 1 and 2, it can be approximately expressed as Δ / r_i . r_i is the length between the crown (or saddle) point in yield line 1 and the corresponding point in yield line 2, as shown in Figure 20-(b). The rotation of saddle and crown yield line

are calculated by arctan(l_c/Δ) and arctan(l_s/Δ), respectivly.

The following assumptions are introduced into the simplified model: (1) the effect of energy loss due to heat generation during impact loading and drop hammer rebound can be ignored ; (2) the strain hardening of steel is not be taken into account; (3) the plastic deformation energy of the steel tube between the plastic lines is not considered.

According to the method above, the local indentation dissipated energy (E_{local}) and equivalent impact force (P_e) from test results of Specimen J14a, J15a, J14b and J35b are listed in Table 2. In order to verify the simplified method, the calculated local indentation dissipated energy (E_{local}) and the calculated equivalent impact force (P_e) were compared with the test results, According to Wang et al. [26], the load bearing capacity (P_u) can be defined as the plateau value of the measured impact force versus time relation curve. It can be seen from Table 2, the calculated local indentation dissipated energies (E_{local}) agree well with the numerical results ($E_{s,local}$) and there is a little difference between the calculated equivalent impact force (P_e) and the measured load bearing capacity(P_u). The difference can be attributed to the assumptions in deduction process. In general, the method can provide a valuable reference for evaluating the impact resistance of steel tubular joint and anti-impact design of steel tubular structures under impact loading.

7. Conclusions

This paper introduces an finite element model to analyze the dynamic behavior of tubular

T-joints subjected to lateral impact loading. A series of tests conducted by the authors are presented to provide information for validation of the FE model and to investigate the buckling mechanism of tubular T-joints under impact loading. A simplified calculation method is proposed to assess the resistance of T-joint under impact loading.

From the results of this paper, the following conclusions may be drawn:

(1). The FEM model can be used to simulate the failure mode and dynamic responses of tubular T-joints subjected to lateral impact loading with good precision. The FE analysis indicates that the tubular joint experiences the coupled local and global deformations during the impact loading.

(2). in the FE model, the failure modes of chord cross section at different time points are captured to decipher the impact force versus time history relation of the tubular T-joint. Seven typical time points in the impact force versus time history curve are identified to highlight the deformational development of the tubular T-joint.

(3). The FE modeling is used to distinguish the local deformation from the global deformation in order to discover the failure mechanism of tubular T-joints under impact loading. The failure mechanism of tubular T-joints is dominantly controlled by the progressive local indentation of steel tube close to the brace-chord connection zone. The failure mechanism also can be verified by the time history of the ratios of the local indentation-dissipated and global bending-dissipated energy to the total plastic deformation energy. Accordingly, the steel tubular T-joint under impact loading is vulnerable to local indentation.

(4). Based on the simplified yield line pattern of the locally-buckled top surface of chord and the reciprocal theorem of work, an equivalent impact force estimation method is developed in

this paper to determine the anti-impact resistance of steel tubular T-joint. It provides an effective method for evaluating the impact resistance of steel tubular joint and anti-impact design of steel tubular structures.

Acknowledge

The work was funded by National Science Fund (51108399), Shandong College and University S&T Planed Projects (J11LE11), Shangdong Science Fund (ZR2011EL046) and the Program for New Century Excellent Talents in University (NCET-11-0123).

The research described in the paper was conducted at the Center for Integrated Protection Research of Engineering Structures (CIPRES), Ministry of Education Key Laboratory of Building Safety and Efficiency of the Hunan University, so particular thanks to the financial support of Project of Ministry of Education Key Laboratory of Building Safety and Energy Efficiency, Hunan University (2012001).

References

[1] Spares CG, Soreide TH. Plastic analysis of laterally loaded circular tubes. J Struct Eng 1983; 109(2): 451-67.

[2] Zeinoddini M, Harding JE, Parke GAR. Effect of impact damage on the capacity of tubular steel members of offshore structures. Mar. Struct 1998; 11(4-5):141-57.

[3] Zeinoddini M, Harding JE, Parke GAR. Dynamic behaviour of axially pre-loaded tubular steel members of offshore structures subjected to impact damage. Ocean Eng 1999; 26(10): 963-78.

[4] Zeinoddini M, Harding JE, Parke GAR. Contribution of ring resistance in the behaviour of

steel tubes subjected to a lateral impact. Int J Mech Sci 2000; 42(12): 2303-20.

[5] Zeinoddini M, Parke GAR, Harding JE. Axially pre-loaded steel tubes subjected to lateral impacts: An experimental study. Int J Impact Eng 2002; 27(6):669-90.

[6] Zeinoddini M, Harding JE, Parke GAR. Axially pre-loaded steel tubes subjected to lateral impacts (a numerical simulation). Int J Impact Eng 2008; 35(11): 1267-79.

[7] Zeinoddini M, Parke GAR, Harding JE. Interface Forces in Laterally Impacted Steel Tubes. Exp Mech 2008; 48(3): 265-80.

[8] Chen KS, Shen WQ. Further experimental study on the failure of fully clamped steel pipes. Int J Impact Eng 1998; 21(3): 177-202.

[9] Bambach MR, Jama H, Zhao XL, Grzebieta RH. Hollow and concrete filled steel hollow sections under transverse impact loads. Eng Struct 2008; 30(10): 2859-70.

[10]Jones N, Birch RS. Low-velocity impact of pressurized pipelines. Int J Impact Eng 2010; 37(2): 207-19.

[11]Jones N. Dynamic energy absorption and perforation of ductile structures. Int J Pres Ves Pip 2010; 87(9): 482-92.

[12] Jin WL, Song J, Gong SF, Lu Y. Evaluation of damage to offshore platform structures due to collision of large barge. Eng Struct 2005; 27(9): 1317-26.

[13]Wang XL, Zhang YC, Wang ZL. Study on collision behavior of K-joint in offshore jacket platform. J Jiangsu University Sci & Tech (natural science edition) 2007; 21(4): 1-6. [in Chinese]

[14] Yu WJ, Zhao JC, Luo HX, Shi JY, Zhang DX. Experimental study on mechanical behavior of an impacted steel tubular T-joint in fire. J Constr Steel Res 2011; 67(9): 1376-85.

[15] Qu H, Zhang Y. Mechanism analysis of impact performance for tubular T-joint. In: 12th international conference on Inspection, Appraisal Repairs & Maintenance of Structures 2010, Yantai, China.Vol:1, 159-62.

[16] Qu H, Chu F. Impact Performance Studies of T-tubular Joint impacted on the Chord. J Ship Mech 2011; 15(11):1306-13. [in Chinese]

[17] Qu H, Zhang Y, Shao YB. Study of impact performance of tubular T-joint. J Ship Mech 2012; 16(1-2):156-64. [in Chinese]

[18] ABAQUS. ABAQUS 6.10, Theory manual and users Manual. Pawtucket USA: HKSHibbitt, Karlsson & Sorensen Inc.; 2010.

[19] Qu H, Huo JS, Xu C. Experimental study on tubular T-joints under drop hammer impact loads. J Build Struct. (in publishing) [in Chinese]

[20] Abramowicz W, Jones N. Dynamic axial crushing of square tubes. Int J Impact Eng 1984; 2(2): 179-208.

[21] GB50017-2013. Code for design of steel structures. China Planning Press. Peking, China (in Chinese).

[22] Ellinas CP. Ultimate strength of damaged tubular bracing members. J. Struct. Eng. 1984; 110(2):245-9.

[23]Mohammad RK, Masoud N. A numerical investigation into strength and deformation characteristics of preloaded tubular member under lateral impact loads. Mar Struct 2012; 25(1): 33-57.

[24] Jones N. An approximate rigid-plastic analysis of shell intersections loaded dynamically. J. of Engineering for Industry, 1973; 95(1): 321-331.

[25]Malvar LJ, Ross CA. Review of strain rate effects for concrete in tension. ACI Mater J 1998; 95(6):735-9.

[26]Wang R, Han LH, Hou CC. Behavior of concrete filled steel tubular (CFST) members under lateral impact: Experiment and FEA model. J Construct Steel Res 2013; 80(1):188-201.

Tables

Table 1 Summary of Test Information **(adopted from reference [19])**

Specimen number	Dimension of chord $D\times T\times L$ (mm)	Dimension of brace $d\times t\times l$ (mm)	α	E_sI_{chord} (10^{12}N.mm^2)	Nature frequency （Hz）	Hammer weight m（kg）	Impact velocity v（m/s）	Impact energy E（kJ）	Impact capacity （kN）	Mid-span residual deflection （mm）
J14a	180×6×1890	89×4×600	21	2.6	102	460	7	11.27	289	45
J15a	180×6×1890	89×4×600	21	2.6	102	590	7	14.5	238	67
J14b	180×6×1890	89×4×600	21	2.6	102	460	10	23	-	110
J35b	325×7×1890	89×4×600	5.8	18.2	176	590	10	29.5	300	51

Table 2 Details of plastic hinge zone and simplified calculation of impact force (adopted from reference [19] partly)

Specimen number	Length of crown yield line r_1/mm	Length of saddle yield line r_2/mm	Dent depth △ /mm	Rotation of yield line 1 and 2 /rad	Rotation of saddle yield line /rad	Rotation of crown yield line /rad	Total length of yield line 1 and 2 /mm	Total length of crown yield line /mm	Total length of saddle yield line /mm	*DIF*	Plastic moment of steel plate of chord M_p/N.mm	Equivalent impact force P_e/kN	Measured bearing capacity P_u/kN	P_e/P_u	Measured local dissipation of energy E_{local}/kJ	Numerical local dissipation of energy $E_{s,local}$/kJ
J14a	51	48	23	0.45	1.45	1.56	1027	101	96	1.33	4491	196	288	0.68	4.5	4.7
J15a	41	48	26	0.58	1.42	1.56	998	81	96	1.34	4491	193	238	0.81	5.0	4.8
J14b	33	78	50	0.99	1.26	1.56	1071	66	156	1.35	4491	165	-	-	8.3	8.5
J35b	71	46	40	0.11	1.48	1.55	1211	336	211	1.41	5451	214	218	0.98	8.6	7.8

Figures

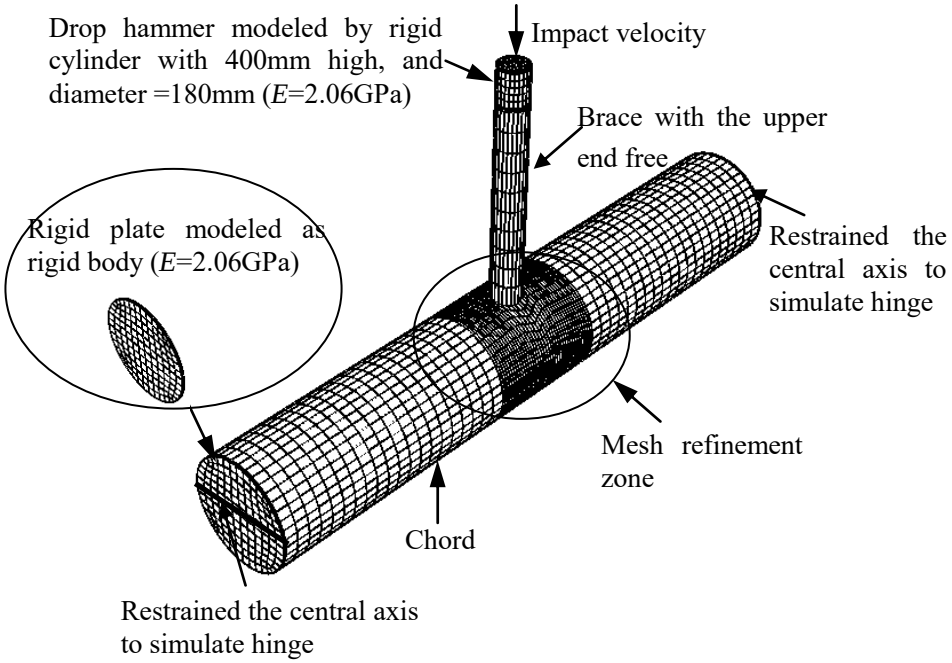

Figure 1 FEA model of T-joint under impact loading

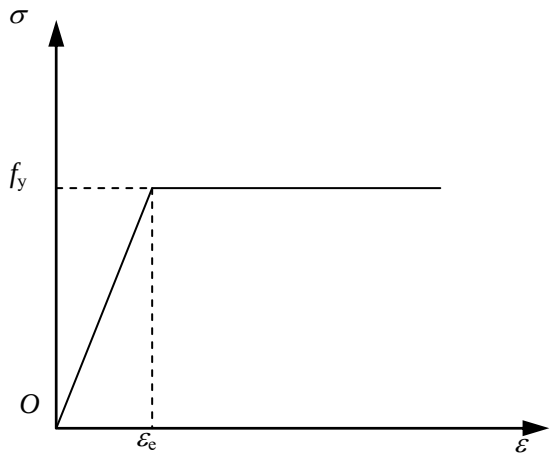

Figure 2 Material model of steel

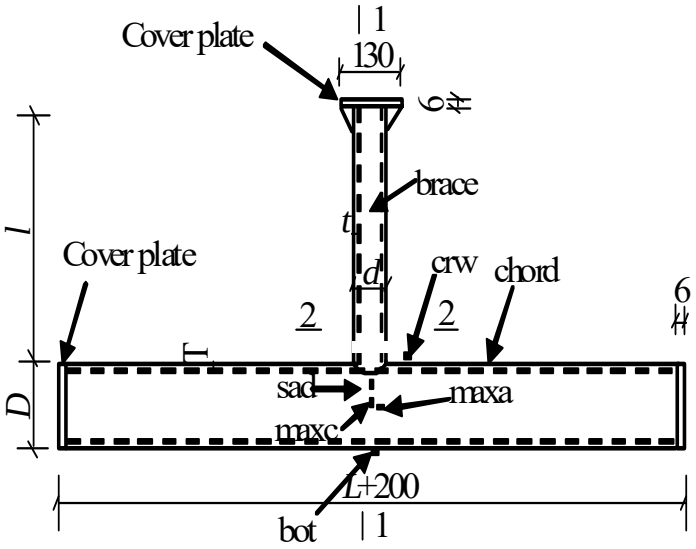

(a) Front view

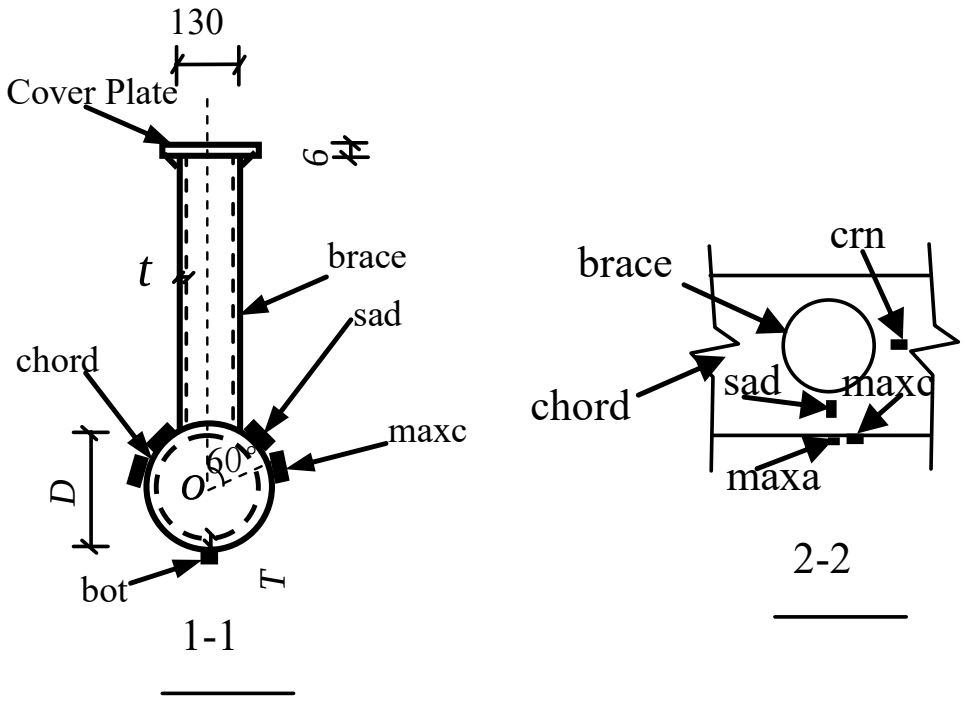

(b) Profile view

Figure 3 Details of specimens and strain gauge layout (unit: mm)

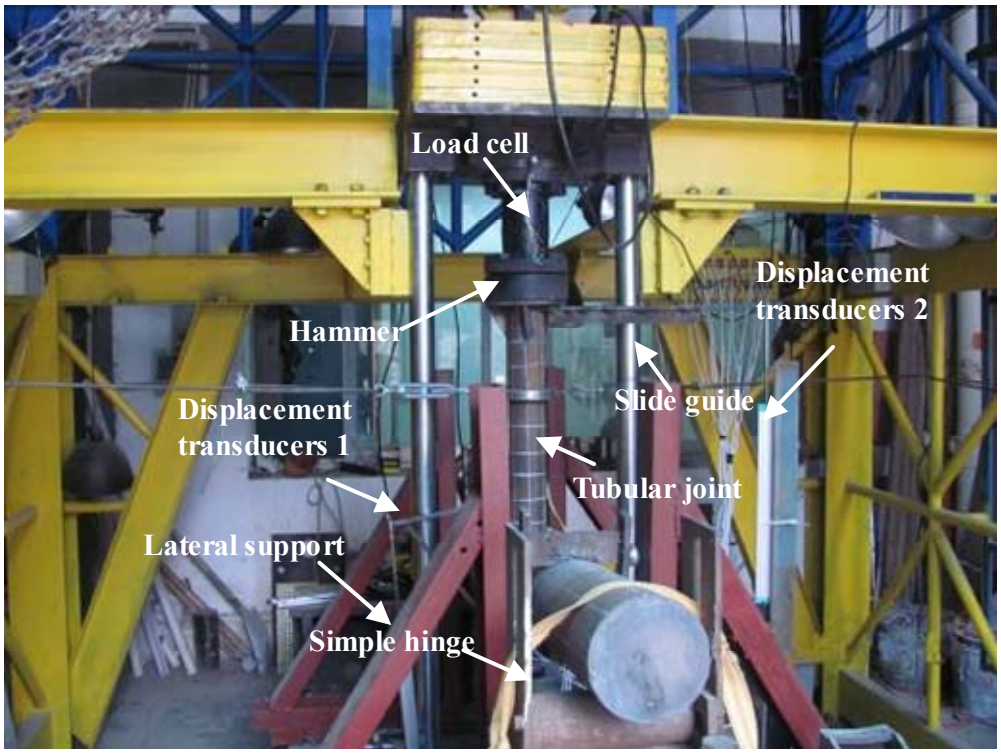

Figure 4 Impact test setup

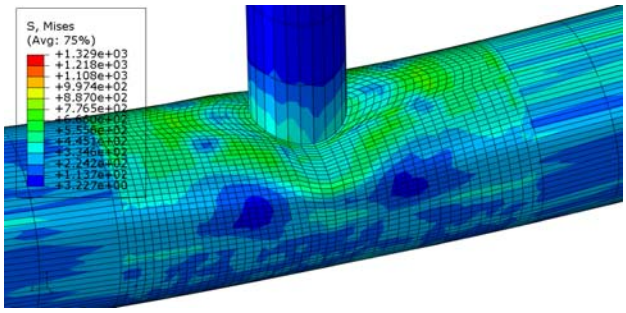

(1) experiment (2) simulation

(a) J14a

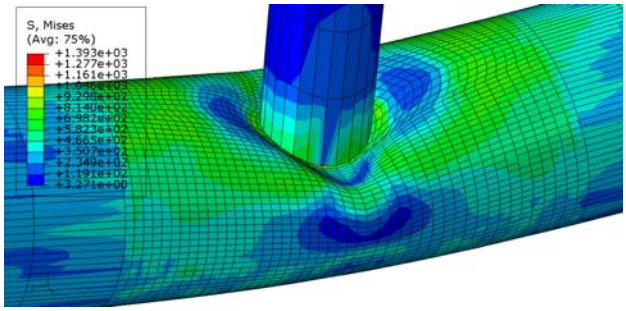

(1) experiment (2) simulation

(b) J15a

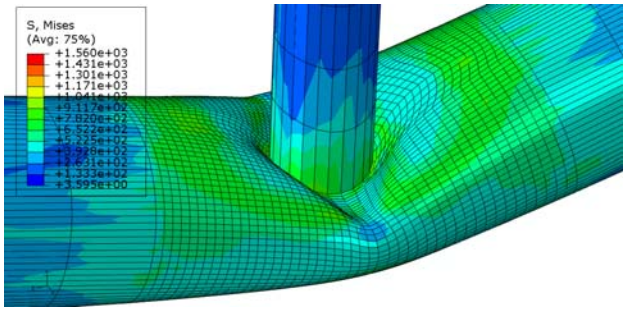

(a) experiment (b) simulation

(c) J14b

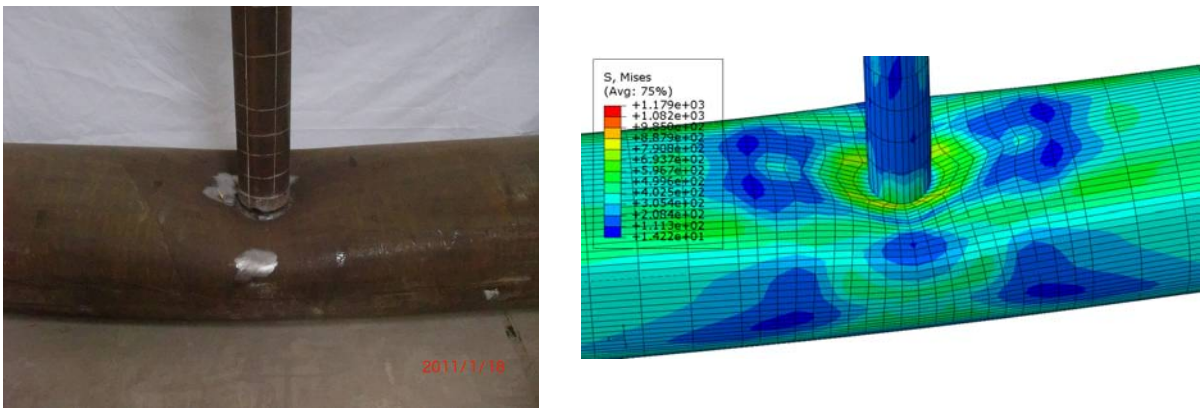

(a) experiment (b) simulation

(d) J35b

Figure 5 Comparisons of failure modes of tested specimens with numerical results

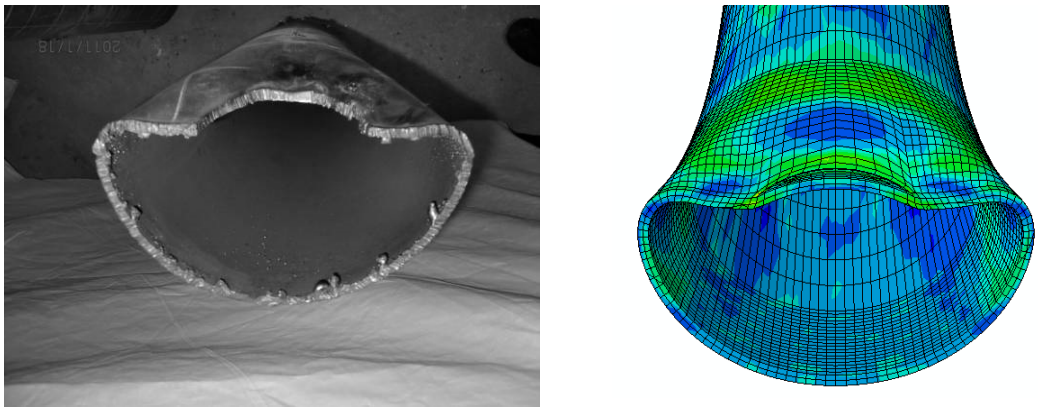

(a) experiment (b) simulation

Figure 6 Comparison of physical failure mode of Specimen J15A with simulated failure mode

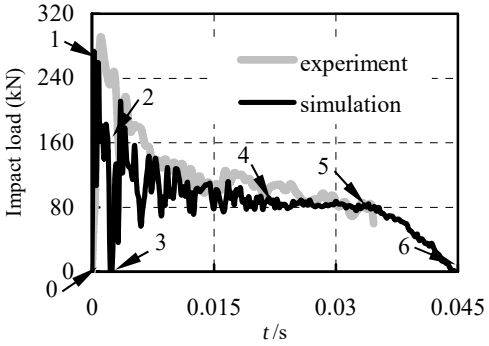

(a) J14a

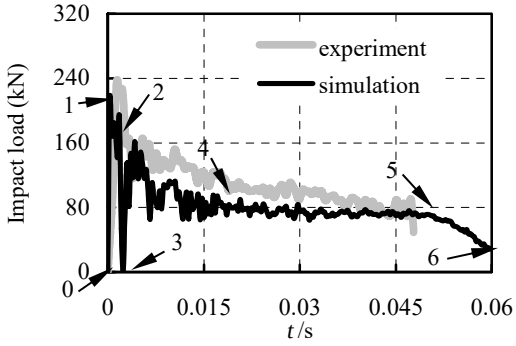

(b)J15a

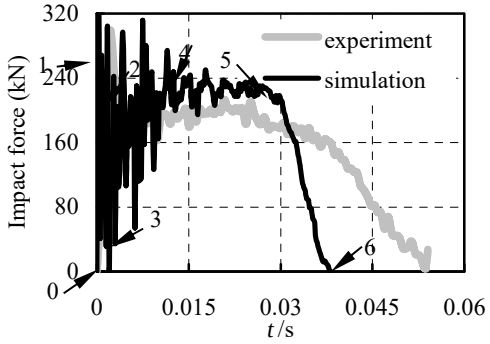

(c) J35b

Figure 7 Comparisons of measured impact load versus time history relations with numerical results

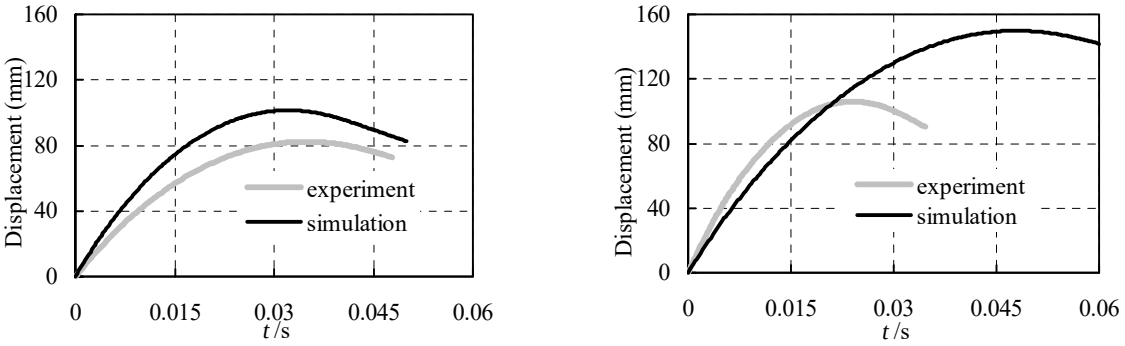

(a) J14a **(b)J15a**

Figure 8 Comparisons of measured vertical displacement versus time history relations with numerical results

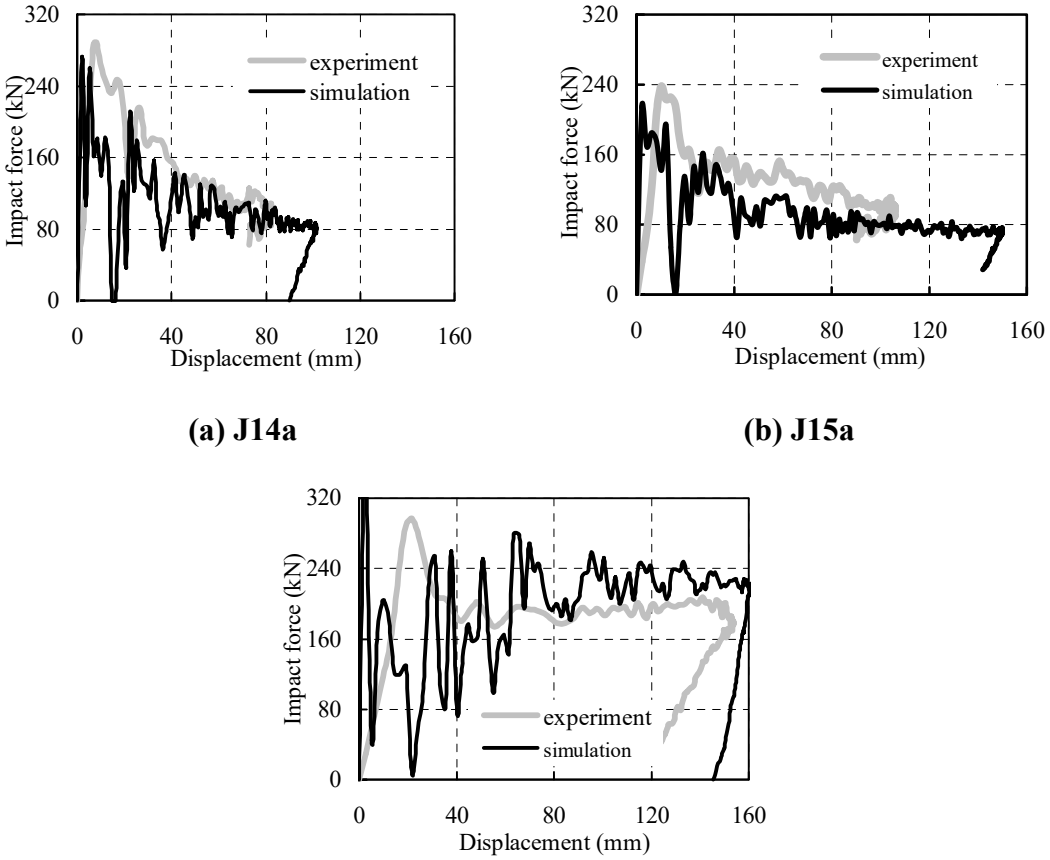

(a) J14a

(b) J15a

(c) J35b

Figure 9 Comparisons of numerical impact force versus displacement curves with tested results

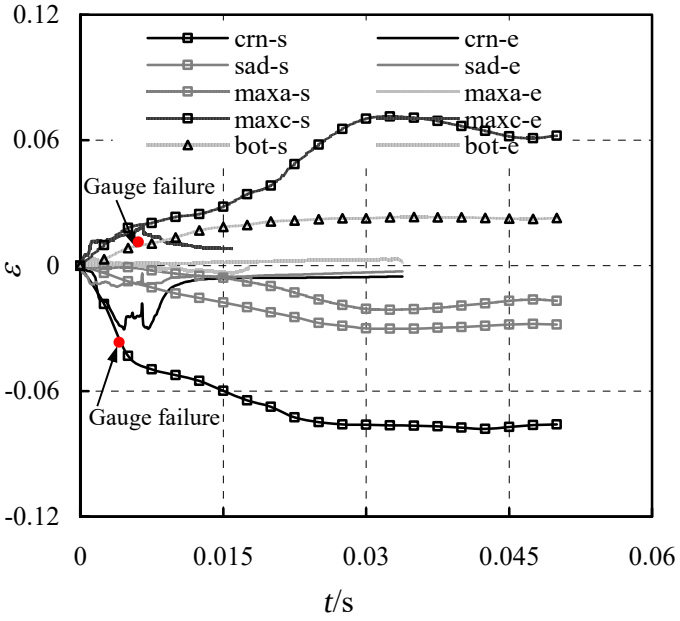

(a) J14a

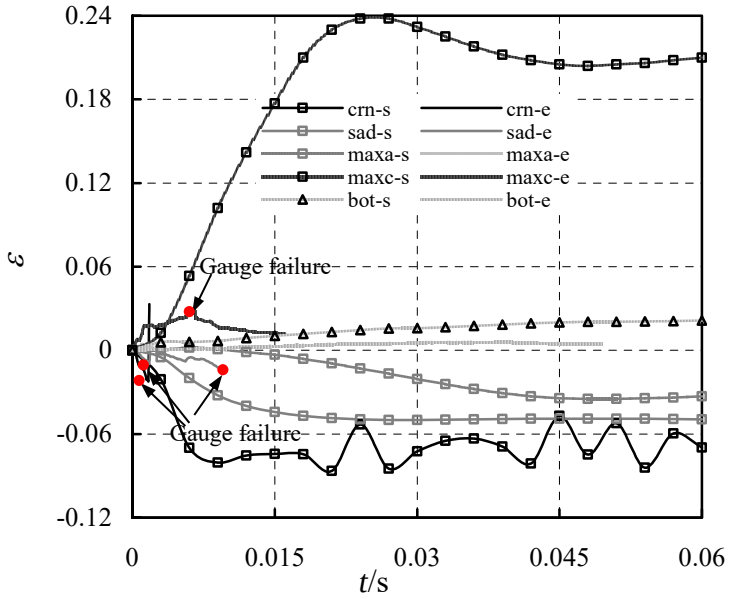

(b) J15a

Figure 10 Comparisons of numerical strain versus time curves with tested results

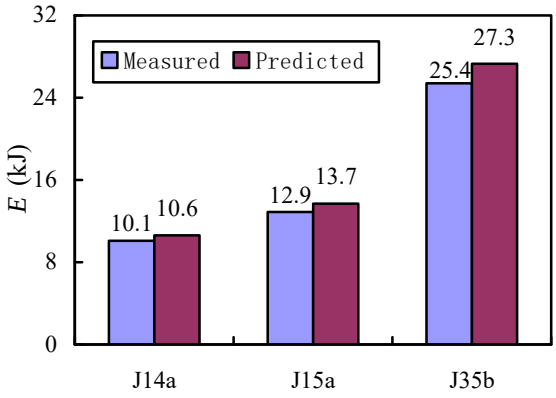

(a) Dissipated energy

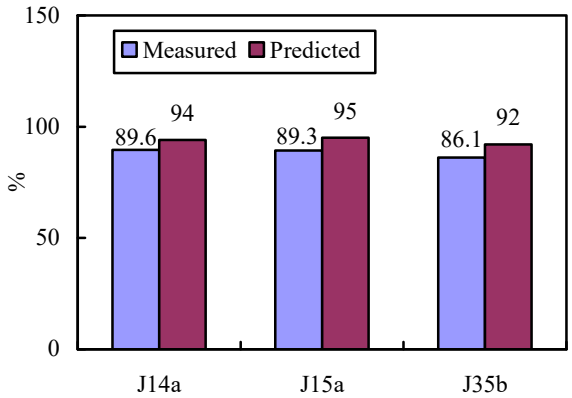

(b) Ratio of dissipated energy to applied impact energy

Figure 11 Comparisons of measured energy dissipation with predicted results

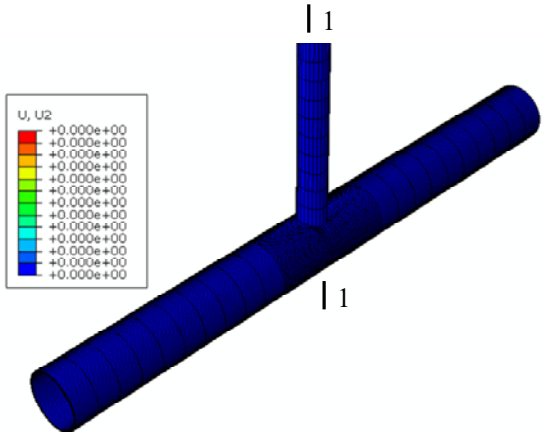

(a) panorama

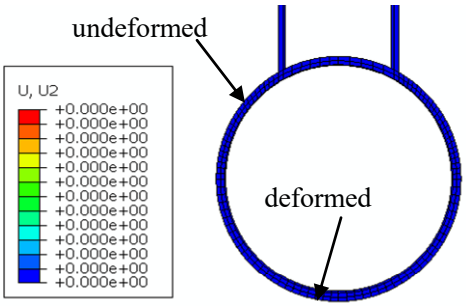

(b) 1-1

(1) *t*=0ms

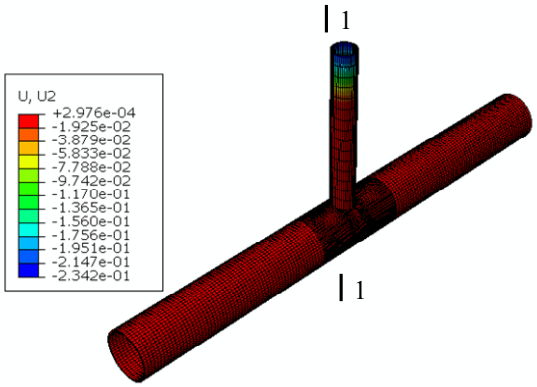

(a) panorama

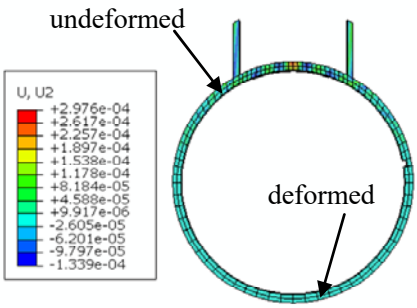

(b) 1-1

(2) *t*=0.25ms

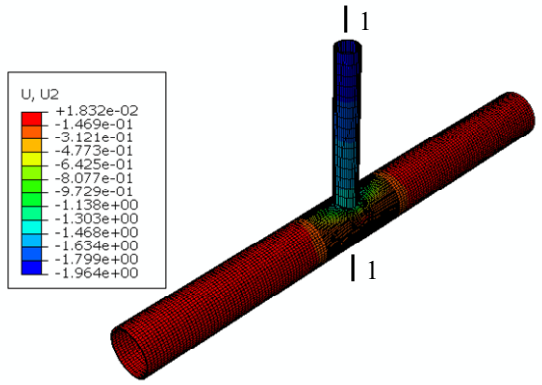

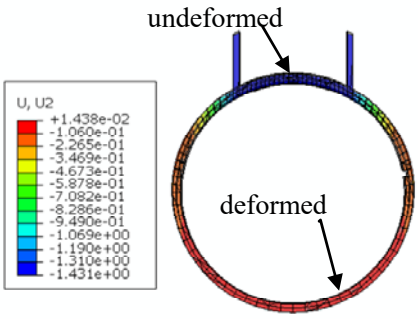

(a) panorama (b) 1-1

(3) *t*=0.5ms

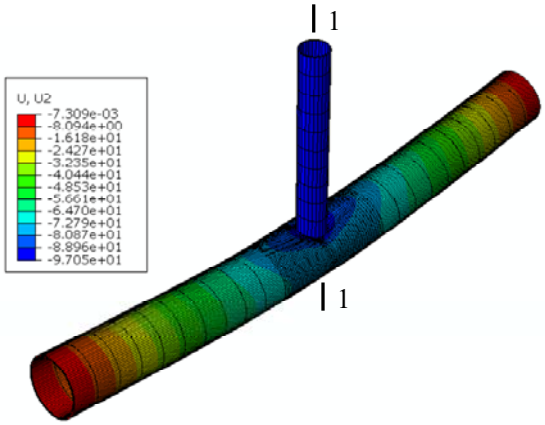

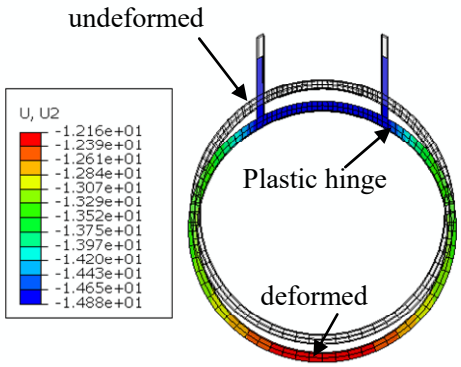

(a) panorama (b) 1-1

(4) *t*=2.5ms

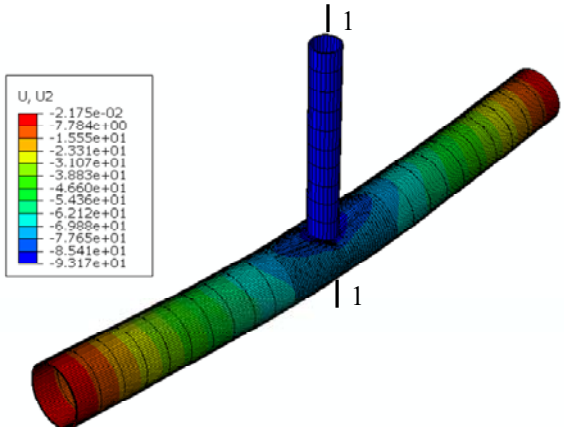

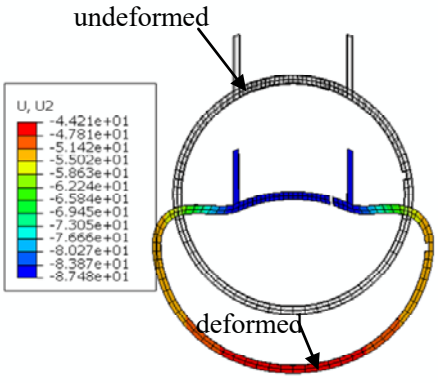

(a) panorama (b) 1-1

(5) *t*=23.5ms

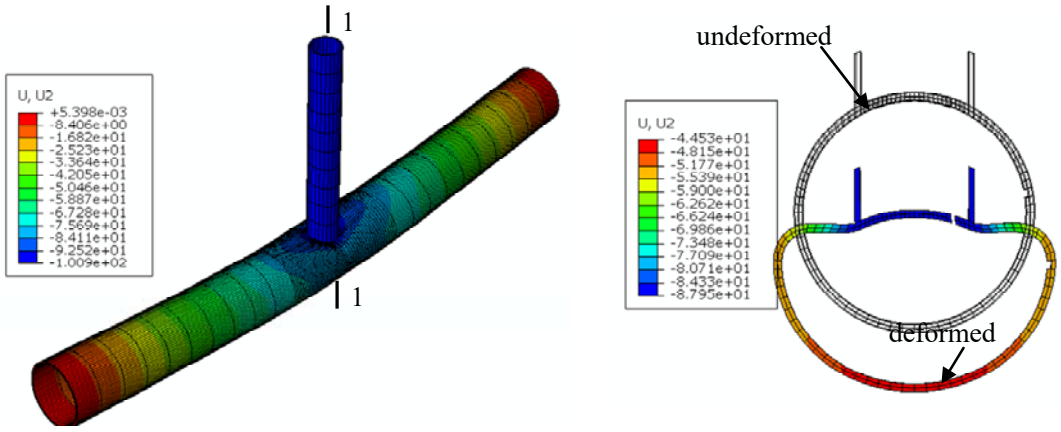

(a) panorama (b) 1-1

(6) *t*=35ms

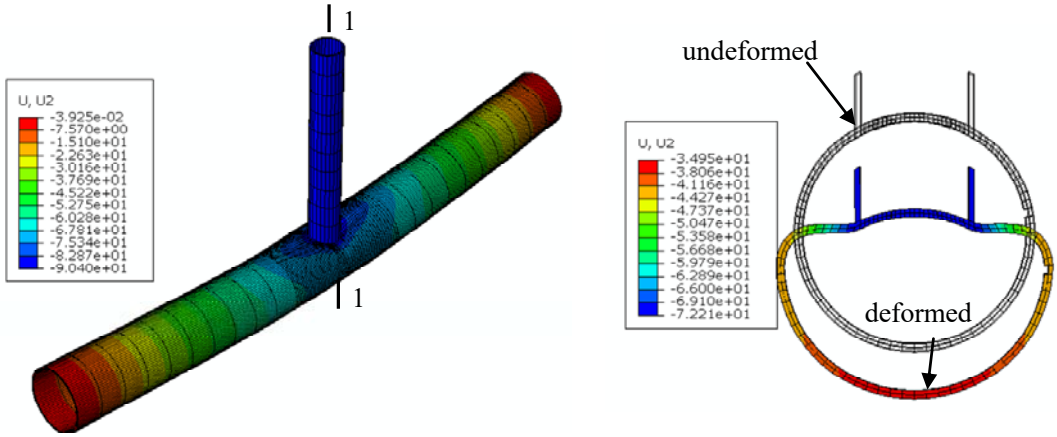

(a) panorama (b) 1-1

(7) *t*=45ms

Figure 12 Failure modes of chord cross section of J14a at different time points (ms)

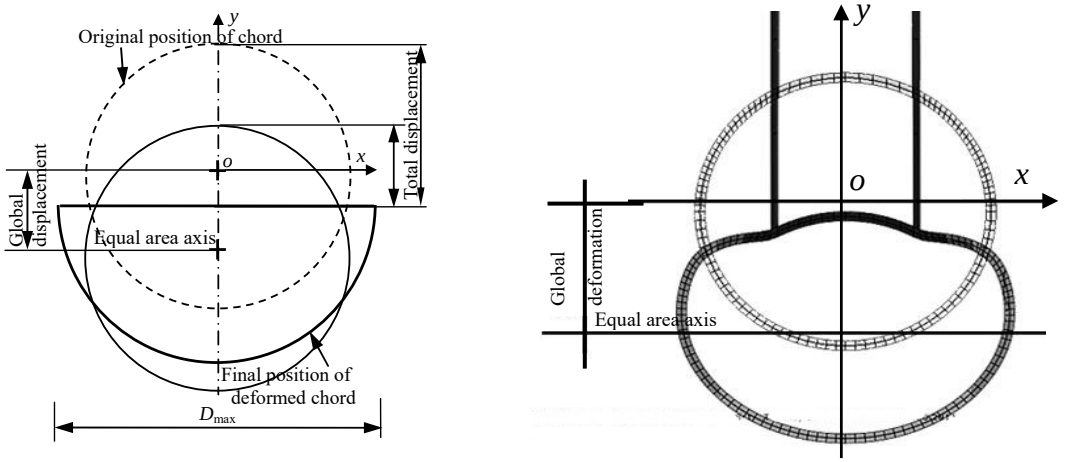

(a) deformation calculation diagram[10] **(b) global deformation of chord**

Figure 13 Definition of global, local and total displacements of chord

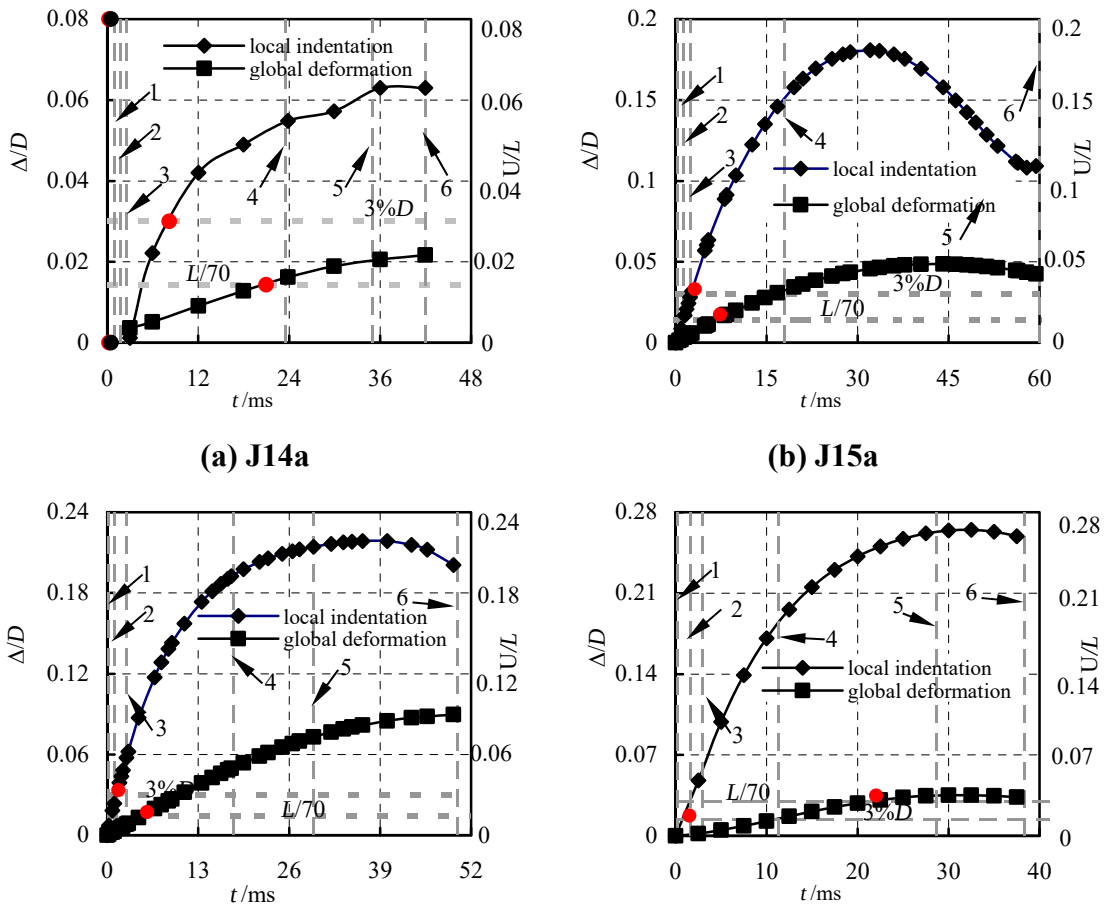

(a) J14a (b) J15a

(c) J14b (d) J35b

Figure 14 Relationship between local and global deformations

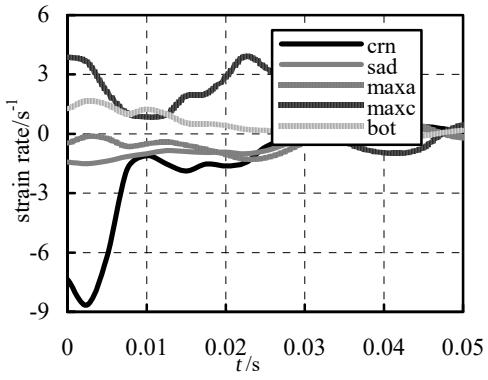

(a) J14a

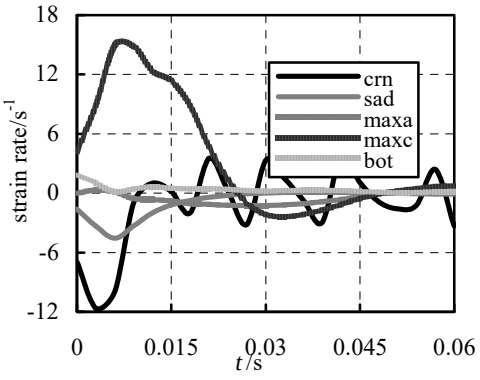

(b)J15a

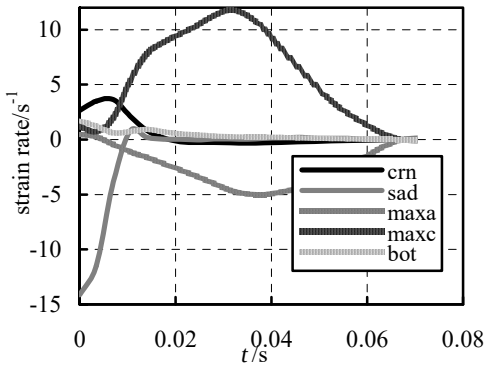

(c) J14b

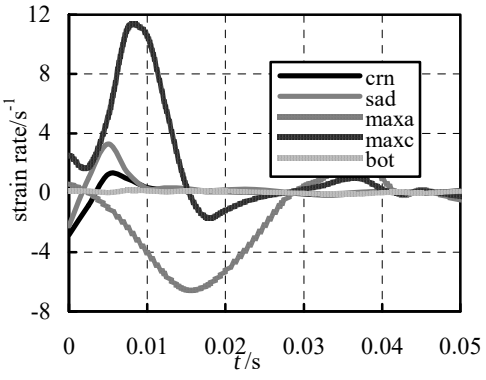

(d) J35b

Figure 15 Strain rate time history curves at typical positions

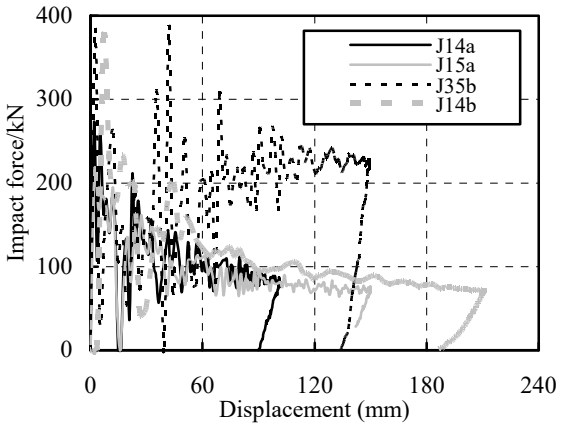

Figure 16 Measured impact load versus displacement curves of Specimens J14a, J14b, J15a and J35b

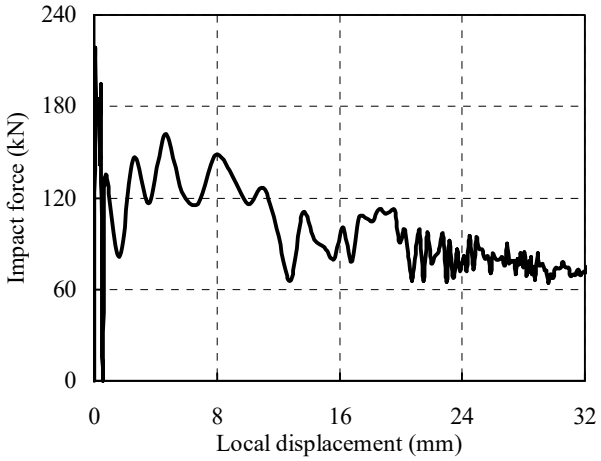

Figure 17 Impact force versus local indentation curve of Specimen J15a

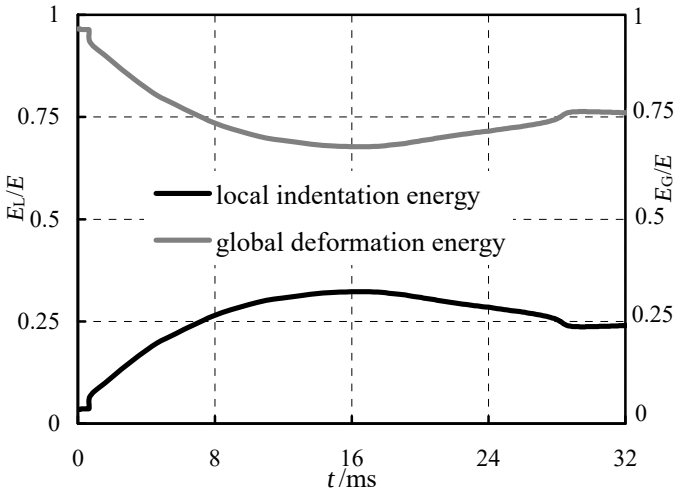

Figure 18 Ratios of local indentation and global bending dissipated energy to total energy versus time history curves of Specimen J15a

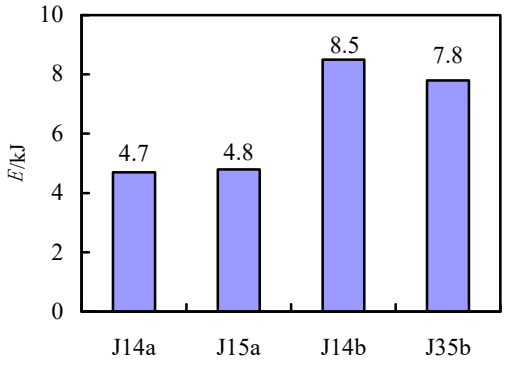

(a) local indentation dissipated energy

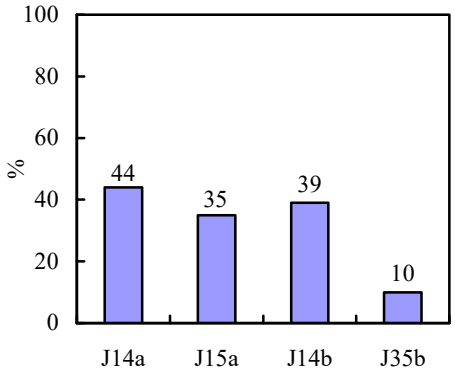

(b) ratio of local indentation dissipated energy to total energy

Figure 19 Analysis of local indentation dissipated energy

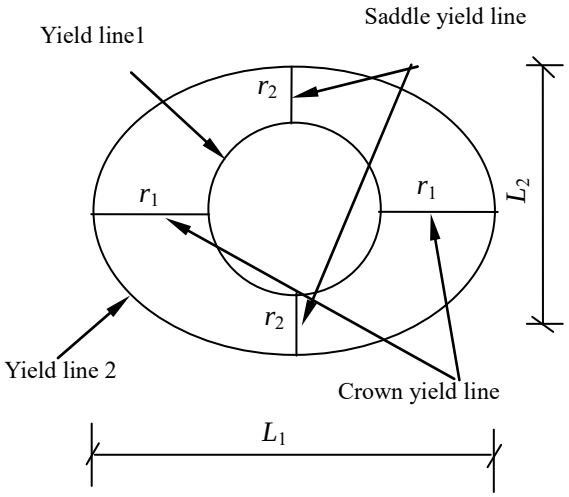

(a) Yield line on plan

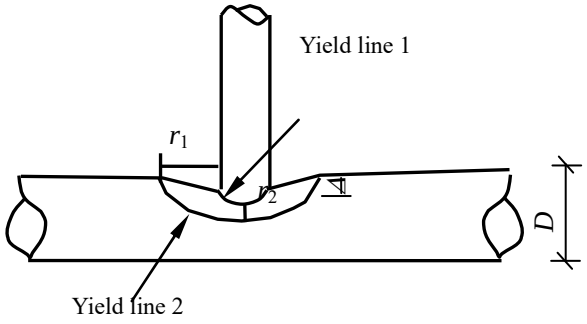

(b) Side elevation

Figure 20 Yield line pattern in local indentation zone